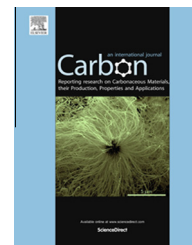


Available at [www.sciencedirect.com](http://www.sciencedirect.com)

ScienceDirect

journal homepage: [www.elsevier.com/locate/carbon](http://www.elsevier.com/locate/carbon)

# Influence of nonionic surfactant-modified PEDOT:PSS on graphene

Jae-Bok Lee <sup>a</sup>, Kuldeep Rana <sup>a</sup>, Byung Hwa Seo <sup>a</sup>, Jin Young Oh <sup>b,c</sup>, Unyong Jeong <sup>b</sup>, Jong-Hyun Ahn <sup>a,\*</sup>

<sup>a</sup> School of Electrical and Electronic Engineering, Yonsei University, Seoul 120-749, Republic of Korea

<sup>b</sup> School of Materials Science and Engineering, Yonsei University, Seoul 120-749, Republic of Korea

<sup>c</sup> Research Institute of Iron and Steel Technology, Yonsei University, Seoul 120-749, Republic of Korea

## ARTICLE INFO

### Article history:

Received 4 October 2014

Accepted 24 December 2014

Available online 2 January 2015

## ABSTRACT

Graphene is a potential candidate for use as the transparent conducting electrode in organic photovoltaics and is emerging as a possible substitute for conventional indium tin oxide-based electrodes. However, challenges such as difficulty in coating other materials on top of graphene and stable doping of graphene have yet to be overcome to improve device performance. Here, we have developed a simple approach to improve the wettability of poly(3,4-ethylene-dioxy-thiophene):poly-(styrenesulfonate) (PEDOT:PSS) polymer on a graphene surface by mixing it with a nonionic small molecule surfactant (Triton X-100). This results in a uniform coating over the graphene surface and simultaneously increases the conductivity via doping effects. The significance of this strategy has been verified in organic photovoltaics on flexible substrates. These photovoltaics on flexible substrate show maximum power conversion efficiency (PCE) values of 3.19%, which are much improved compared to photovoltaics with pristine graphene electrodes (1.12%).

© 2015 Elsevier Ltd. All rights reserved.

## 1. Introduction

Since its discovery, graphene has attracted much attention due to its novel and remarkable physical properties, which make it the material of choice for many applications compared to other two-dimensional materials [1]. Monolayer graphene has outstanding characteristics such as superior optical transparency (absorbs only 2.3% of visible light), exceptional electrical conductivity, and mechanical flexibility [2–6]. These properties make it highly suitable for the transparent conducting electrode material in organic photovoltaics (OPVs) to replace widely used indium tin oxide (ITO), which has several drawbacks such as poor flexibility, high cost and complicated manufacturing process. In addition to the

transparent conducting electrode, it can be used in a diverse range of device component such as active and interfacial layer as well. Flake forms of graphene have been also studied as an alternative electrocatalyst in dye sensitized solar cell [7,8] and an additive to improve the charge selectivity of active layer in OPV [9,10]. The potential applications of graphene in OPVs depend on surface wettability, which is related to the morphology and the chemical composition of the graphene surface. It is difficult to successfully spread other materials on the chemical vapor deposition (CVD) graphene due to its low surface energy [11–13]. It is challenging to obtain a uniform coating of an aqueous solution of poly(3,4-ethylene-dioxythiophene):poly-(styrenesulfonate) (PEDOT:PSS) on the graphene surface, which is hydrophobic in nature [14,15].

\* Corresponding author.

E-mail address: [ahnj@yonsei.ac.kr](mailto:ahnj@yonsei.ac.kr) (J.-H. Ahn).

<http://dx.doi.org/10.1016/j.carbon.2014.12.101>

0008-6223/© 2015 Elsevier Ltd. All rights reserved.

Several approaches have been reported to resolve the issue of the coating problem of PEDOT:PSS on the hydrophobic graphene surface. Surface treatments through ultraviolet (UV) exposure can help in making its surface from hydrophobic to hydrophilic due to the formation of –OH functional groups [16]. However, the main drawback of UV treatment is it can severely degrade the graphene surface and adversely affects its electrical properties. Further, in order to reduce the surface tension of PEDOT:PSS, a nonionic fluoro-surfactant polymer (Zonyl) has been used [17,18]. In this case, extra additives, such as dimethyl sulfoxide (DMSO) and ethylene glycol (EG), are required to enhance the conductivity, which are unstable under large strains. Molybdenum trioxide has also been used as a buffer layer to improve the wettability of the PEDOT:PSS over the graphene surface [19–21]. However, the performance of OPVs with these modifications is still much lower than those fabricated with ITO electrodes.

As discussed above, the main problems associated with these approaches are the hydrophobic nature and low surface energy of graphene which prevent the uniform dispersion of PEDOT:PSS onto the graphene surface. Even though the coating problem of graphene surface has been improved by various efforts, there are a few more areas of concern such as degradation in property and additional processing steps, which are still needed to be resolved. Here, we have introduced a simple method of uniform coating of the aqueous PEDOT:PSS onto the hydrophobic graphene surface by mixing a nonionic small molecule surfactant, Triton X-100, (polyethylene glycol p-(1,1,3,3-tetramethylbutyl)-phenyl ether), with PEDOT:PSS which makes the long nanofibril structure of hydrophobic PEDOT [22]. This modified PEDOT:PSS, which can be uniformly coated on the graphene surface without any additional treatment, simultaneously acts as a source of p-doping for graphene. This doping results mainly from the electron transfer from the graphene to the PEDOT:PSS due to the sulfonic group of PSS acidic chain as well as the work function difference between graphene and PEDOT:PSS as well reported in previous studies [23,24]. Thus, we have optimized the concentration of Triton X-100 in PEDOT:PSS for better coating, which led to an improvement in the electrical properties and passivation during stretching. To illustrate the advantages of this coating method, which yields improved mechanical stability under strain and conductivity in the modified PEDOT:PSS, graphene electrode (sheet resistance of  $\sim 90 \Omega/\text{sq}$ )-based OPVs with improved efficiency have been fabricated for testing.

## 2. Experimental section

### 2.1. Graphene electrode preparation

Graphene was synthesized by the well-known CVD method on a copper substrate. The copper foil (25  $\mu\text{m}$  thick) was inserted in the middle of a quartz tube furnace at low pressure and annealed at 1000 °C for 2 h and 40 min under the injection of 10 sccm of hydrogen ( $\text{H}_2$ ). After the annealing process, 1 sccm of methane ( $\text{CH}_4$ ) as a carbon source was flowed and the temperature was maintained for 5 h and 30 min. Finally, the furnace was cooled down to room temperature

in the presence of  $\text{H}_2$ . In order to fabricate the graphene electrode, polymethyl methacrylate (PMMA) was first coated on one side of the graphene-covered copper foil, which acts as a supporting layer and the copper was etched away using a 0.1 M ammonium persulfate solution. The graphene film supported by the PMMA was transferred onto a polyethylene terephthalate (PET) substrate. After drying the transferred sample, the supporting layer was removed by dissolution in acetone. By repeating this transfer process, a transparent, high quality, multi-layered graphene electrode was prepared.

### 2.2. Organic photovoltaic fabrication

As-received PEDOT:PSS (Clevios AI 4083) which has low conductivity (10  $\text{k}\Omega/\text{sq}$ ) without any additives for conductivity, was modified with 1 wt% of Triton X-100. 1 wt% is an optimized concentration for uniform coating on hydrophobic graphene surface. The modified PEDOT:PSS was filtered by a 0.45  $\mu\text{m}$  PVDF syringe filter and spin-coated on top of five-layer stacked graphene at a maximum speed of 4000 rpm for 60 s. These PEDOT:PSS-coated graphene samples were dried at 150 °C for 30 min and then transferred into a glove box to spin-coat the active layer. A blended solution of poly(3-hexylthiophene-2,5-diyl) (P3HT) and phenyl-C61-butyric acid methyl ester (PCBM) (20  $\text{mg}/\text{mL}$ ), which was composed of the same weight fraction in dichlorobenzene for the bulk heterojunction layer, was filtered with a 0.2  $\mu\text{m}$  PTFE syringe filter and coated on the PEDOT:PSS layer at a speed of 600 rpm for 60 s. After drying the sample on a hot plate at 150 °C for 30 min, the top electrodes (20 nm of calcium and 200 nm of aluminum) were thermally evaporated using a shadow mask. Finally, the performances of devices were examined under 100  $\text{mW}/\text{cm}^2$  illuminations using a solar simulator.

## 3. Results and discussion

Fig. 1(a–c) show the optical microscope images of the graphene surface after coating with different concentrations of Triton X-100 in the PEDOT:PSS. Fig. 1(a) shows the non-uniformly coated surface of the aqueous PEDOT:PSS solution over the graphene surface, which is due to the hydrophobic nature of the surface. The dark area is covered with the PEDOT:PSS while the remaining portion is uncoated graphene. As the concentration of the Triton X-100 is increased, the wettability of the PEDOT:PSS on the graphene is improved. When 0.5 wt% of Triton X-100 is added to the PEDOT:PSS solution, the uniformity of the coating is improved; however, complete coverage of the graphene surface is still not achieved (as shown in Fig. 1(b)). Fig. 1(c) shows the uniformly covered surface of the graphene when 1 wt% of Triton X-100 was mixed into the PEDOT:PSS solution. Adding Triton X-100 not only addresses the coating uniformity problems but also improves the electrical properties of the PEDOT:PSS and graphene by forming a 15–20 nm nanofibril structure of hydrophobic and conductive PEDOT, as shown in the atomic force microscope (AFM) images in Fig. S1. The large amount of PEDOT nanofibril can directly contact the graphene surface and act as a p-type dopant in the graphene. Fig. 1(d) shows the effects of Triton

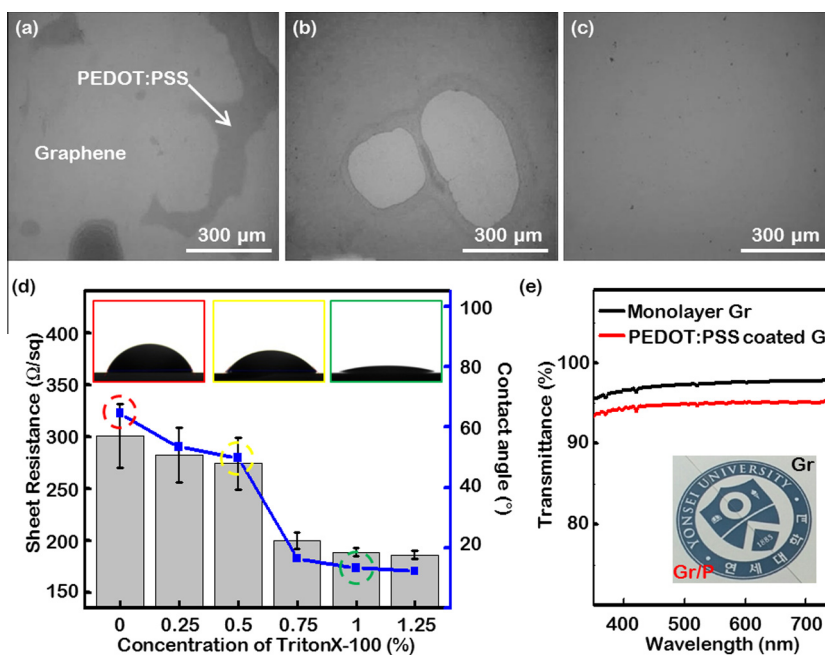


**Fig. 1 – (a–c) Optical microscopy images of PEDOT:PSS coated on the hydrophobic surface of graphene depending on the concentration of Triton X-100, 0%, 0.5% and 1% in order. (d) The sheet resistance of composite films, PEDOT:PSS on graphene, and the contact angle variation of PEDOT:PSS droplet on graphene, depending on the concentration of Triton X-100. The inset images are the PEDOT:PSS droplet on graphene with the 0% (red), 0.5% (yellow) and 1% (green) Triton X-100. (e) Optical transmittances of monolayer graphene and modified PEDOT:PSS coated on the graphene. The inset shows the transparency of both films. (A color version of this figure can be viewed online.)**

X-100 on the interactions between PEDOT:PSS and graphene. As the Triton X-100 concentration is increased, the electrical properties of the composite films, PEDOT:PSS on graphene, are improved. This is confirmed by measuring the sheet resistance, which does not change any further when extra surfactant above 1 wt% is added. Moreover, in order to investigate the interaction between the PEDOT:PSS and graphene, the contact angles of PEDOT:PSS on the graphene depending on the amount of added Triton X-100, are measured and compared. This indicates that the wettability of the PEDOT:PSS solution is improved by adding the Triton X-100, as shown in the inset images of Fig. 1(d), corresponding to 0%, 0.5% and 1% in order. The contact angle is decreased from 64.6° to 13.3° as the concentration of Triton X-100 is increased, and then becomes saturated after 1 wt%. Due to the fact that graphene is hydrophobic, this contact angle variation indicates that the PEDOT:PSS becomes more hydrophobic as Triton X-100 is added (up to 1 wt%) to have good interaction with graphene. Thus, it is confirmed that adding 1 wt% of Triton X-100 into the PEDOT:PSS solution yields the most suitable conditions for the uniform coating of the hydrophobic graphene surface. The optical transmittances of the Triton X-100-treated PEDOT:PSS on graphene and the pristine monolayer graphene are compared in Fig. 1(e). The modified PEDOT:PSS absorbs only ~1% of visible light at a wavelength of 550 nm. The inset image also indicates that treating PEDOT:PSS does not significantly degrade the transmittance.

Fig. 2 shows the electrical properties of graphene after treatment with optimized condition of Triton X-100 on the

PEDOT:PSS solution. The sheet resistances of various samples are measured by the Van der Pauw method, including pristine graphene, pure PEDOT:PSS on monolayer graphene, Triton X-100 on graphene, and Triton X-100-modified PEDOT:PSS on graphene (as compared in Fig. 2(a)). Even though the PEDOT:PSS is conductive, the sheet resistance of the PEDOT:PSS on graphene is not effectively improved due to the poor interface between pure PEDOT:PSS and graphene without any treatment. In addition, since Triton X-100 is a non-ionic small molecule (a nonconductive compound), only the Triton X-100 actually degrades the sheet resistance of the graphene a little. However, the sheet resistance of the Triton X-100-modified PEDOT:PSS (with the optimized weight fraction) on the graphene is improved by about 40%, as compared to the pristine graphene. This increase in performance is due to the doping effect of PEDOT:PSS on the graphene. Fig. 2(b) shows the sheet resistance of graphene on a PET substrate as a function of the number of graphene layers. As it has been demonstrated previously, the sheet resistance decreases (from 309.6 to 92.3 Ω/sq) as the number of graphene layers increases. After the modified PEDOT:PSS is coated on the graphene, the sheet resistance further decreased to 56.3 Ω/sq (for the five-layer stacked graphene). The doping effect of the PEDOT:PSS works efficiently at the top layer of graphene, which is in direct contact with PEDOT:PSS. To verify the surficial doping of PEDOT:PSS, we examined the doping efficiency of Triton X-100-modified PEDOT:PSS on two layers of graphene with different stacking orders. One was modified PEDOT:PSS coated on double-layer stacked

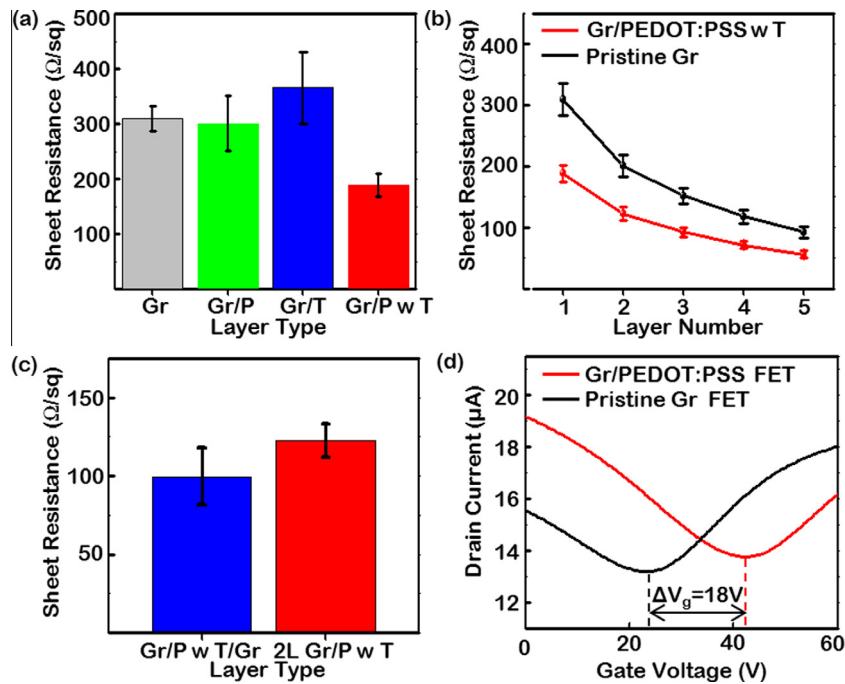


**Fig. 2** – (a) The sheet resistance of each layer: graphene, graphene/PEDOT:PSS, graphene/Triton X-100, and graphene/PEDOT:PSS with Triton X-100. (b) The sheet resistance of graphene depending on the graphene layer before and after doping. (c) The structural doping effect on graphene. (d) The transfer characteristics of graphene channel field-effect transistors before (black) and after (red) coating with PEDOT:PSS (at a drain voltage of 0.1 V). (A color version of this figure can be viewed online.)

graphene and the other was modified PEDOT:PSS sandwiched between two monolayer graphenes. In the latter case, the upper graphene is contacted with the PEDOT:PSS not by spin-coating but via physical Van der Waals forces, which represents a weaker adhesion between the upper graphene and PEDOT:PSS compared to the adhesion between the bottom graphene and PEDOT:PSS. Owing to the different interactions at each interface, the doping effect is not increased by a factor of two (the theoretical value) but still effective compared to the first case. The sheet resistance of the second case is lower (99.7  $\Omega/\text{sq}$ ), compared to the first case (122.4  $\Omega/\text{sq}$ ). For quantitative analysis on the doping of graphene by PEDOT:PSS, graphene channel field-effect transistors were fabricated to investigate the Dirac voltage ( $V_{\text{Dirac}}$ ) shift. In Fig. 2(d), transfer curves are plotted before and after the modified PEDOT:PSS coating on the graphene. The transferred carrier concentration from PEDOT:PSS to graphene can be estimated using the following equation:

$$n = C_{gs} \Delta V_{\text{Dirac}} / q \quad (1)$$

where  $C_{gs}$  is the capacitance between the channel and gate per unit area and  $q$  is the unit charge. In the transfer curves of the fabricated field-effect transistors, the  $V_{\text{Dirac}}$  is shifted to higher voltages by 18 V when pristine graphene is replaced by the modified PEDOT:PSS-coated graphene. The corresponding hole doping concentration was calculated and the doping level reached up to  $1.26 \times 10^{12} \text{ cm}^{-2}$ , which is comparable with previously reported values [1,25–27]. This type of charge transfer is caused by the difference in the work functions and indicates that the PEDOT:PSS is acting as a p-type dopant on the graphene [24].

As reported, nanofibrils have advantage in durability at large strain [22]. The stretching test of pristine (black curve) and modified PEDOT:PSS-coated graphene (red curve) were conducted between 0.1% and 1% with repeated loading and unloading the strain at intervals of 0.1% strain after being transferred onto a PDMS substrate, as shown in Fig. 3(a). These curves are compared in Fig. 3(b). It can be seen that the stacked, multilayer graphene can endure a higher strain than the monolayer graphene because the top graphene layer can supply an additional current path by covering the defects of the bottom layer. The interlayer sliding in between stacked graphene layers also improves the mechanical properties of the multilayer graphene. However, the slope of the red graph is smaller than the black, indicating that the resistance of the graphene coated with PEDOT:PSS is not degraded as much during stretching. This is caused by the passivation of the PEDOT:PSS. This passivation effect of PEDOT:PSS on graphene is presented for various cases ranging from monolayer graphene to five-layer stacked graphene. When 0.1% strain was applied, the sheet resistance of the pristine monolayer graphene increased by 3.3%; this increase is only 0.6% for the graphene coated with the modified PEDOT:PSS. The mechanical properties were further improved when the five-layer stacked graphene was uniformly coated with PEDOT:PSS and a strain of 0.1% was applied. The sheet resistance of the pristine graphene increased by 0.4% compared to the initial value, but that of the modified PEDOT:PSS-coated graphene only increased by 0.2% (compared to the initial value). Thus, the mechanical stability of graphene coated with the modified PEDOT:PSS was improved compared to the pristine graphene; this is similar to the improved sheet resistance values of

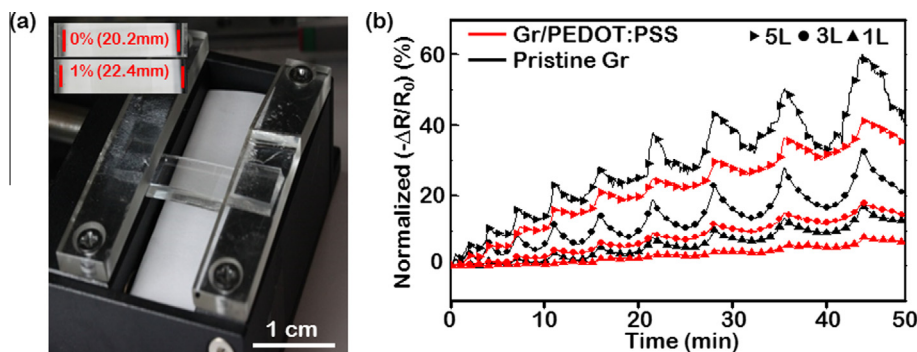


**Fig. 3 – (a) Photograph of the stretching test system for graphene. The inset shows the lowest strain state (0%) and the highest strain state (1%). (b) The stretching test of graphene (black) and modified PEDOT:PSS-coated graphene (red) with repeated loading and unloading the strain at the intervals of 0.1% strain. From the top, the two graphs are measured using the same number of graphene layers: 1, 3, and 5 layers, respectively. (A color version of this figure can be viewed online.)**

coated graphene as compared to the pristine graphene film. This can be related to the nanofibril microstructure of the coated polymer over the graphene, which can preserve the electronic properties under harsh stretching conditions, as mentioned and shown in Fig. S1.

The interaction of graphene with the modified PEDOT:PSS was investigated by Raman spectroscopy in order to understand the doping effect. These spectra are presented as black and red lines, respectively, in Fig. 4(a). In the black graph, the G and 2D band positions are found around  $1586$  and  $2681$   $\text{cm}^{-1}$ , respectively, and the D band, which is generally observed at  $1350$   $\text{cm}^{-1}$ , is almost absent. This indicates the defect-free, high quality of the graphene. Moreover, the positions of the G and 2D peaks and the peak ratio of the 2D peak to the G peak confirm the high-quality of the monolayer graphene. In the red graph, there is a small shift in the PEDOT:PSS peak to  $1439$   $\text{cm}^{-1}$  from the main peak ( $1435$   $\text{cm}^{-1}$ ) due to the effect of Triton X-100. The change in the Raman spectrum of graphene can also be clearly seen as the G and 2D band shifts toward higher wave numbers. The shifts in peak positions of the G and 2D peaks are plotted with respect to the concentration of Triton X-100 in the PEDOT:PSS. These

are represented with different colors: red for the G peak and blue for the 2D peak, as shown in Fig. 4(b). The maximum shift in the G and 2D peaks are about  $10$  and  $5$   $\text{cm}^{-1}$ , respectively, after  $1$  wt% Triton X-100 has been added. These peak shifts are related to charge transfer and are well-matched with the carrier calculation results shown in Fig. 2(d). Similar changes in the Raman spectra have been reported previously, where the G and 2D positions have been shifted by  $10$ – $16$   $\text{cm}^{-1}$ . Corresponding improvements in the sheet resistance (improvements up to  $50$ – $60\%$ ) have also been observed, which are caused by the doping effect [3,28,29].

In order to investigate the potential advantages of well-coated graphene with improved electrical characteristics as transparent conducting electrodes, OPVs have been fabricated on the flexible PET substrates. These devices were fabricated by consecutive coatings and thermal evaporation of PEDOT:PSS, P3HT:PCBM and Ca-Al on the PET/graphene electrode, in which the P3HT:PCBM blend is used as the photo-active layer of the OPV. Fig. 5(a) shows an image of the OPV on a PET substrate, and the inset shows the different layers of the OPV structure. Fig. 5(b) displays the J-V characteristics obtained from the OPVs using different number of

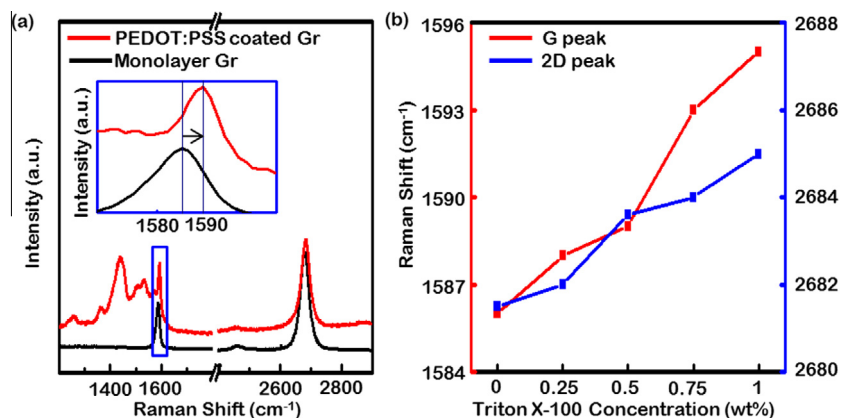


**Fig. 4 – (a) Raman spectra of pristine graphene (black) and modified PEDOT:PSS-coated graphene (red), inset shows the enlarged view of shift in G band of graphene before and after treatment of Triton X-100 on PEDOT:PSS. (b) The positions of the G peak and the 2D peak, as a function of the Triton X-100 concentration, indicate the PEDOT:PSS doping effect on graphene. (A color version of this figure can be viewed online.)**

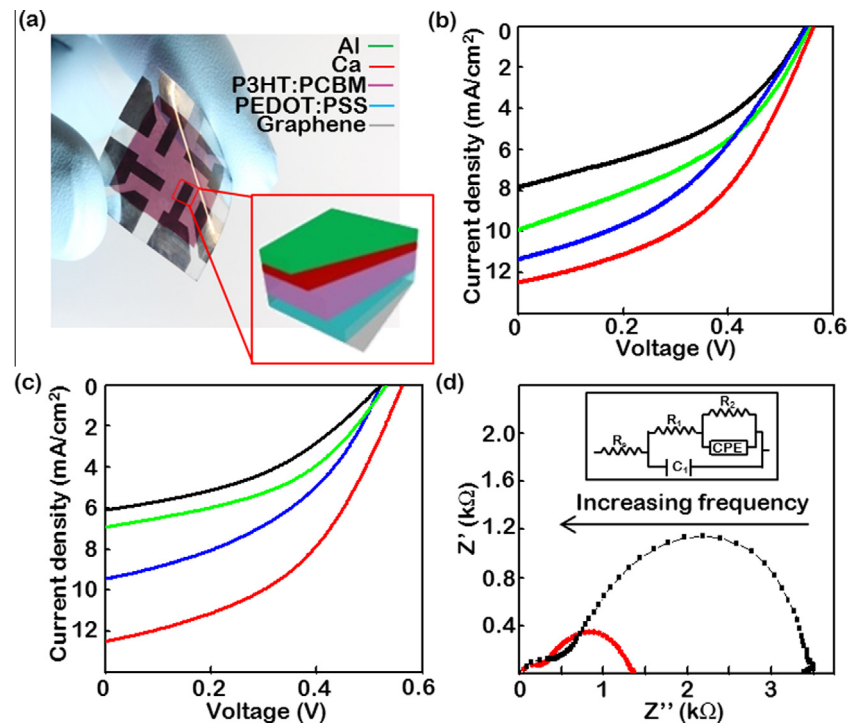


**Fig. 5 – (a) Image of a flexible device. The inset presents the structure of the organic photovoltaic with graphene electrodes. (b) Output curves for the organic photovoltaics with modified PEDOT:PSS depending on their number of graphene layers: from 2 layers (black) to 5 layers (red). (c) Organic photovoltaic output curves using various processing methods to improve the efficiency, including pristine five-layer graphene and pure PEDOT:PSS (black); UV-treated five-layer graphene and pure PEDOT:PSS (green); nitric acid-doped and UV-treated five-layer graphene and pure PEDOT:PSS (blue); and pristine five-layer graphene and Triton X-100-treated PEDOT:PSS (red). (d) Impedance spectroscopy of organic photovoltaics with and without Triton X-100. Inset is the equivalent circuit corresponding to the impedance spectroscopy. (A color version of this figure can be viewed online.)**

layers of graphene electrodes with modified PEDOT:PSS. The J–V characteristics show that the current density increases as more graphene layers are added, which is related to the decreasing sheet resistance of the graphene electrodes, as shown in Fig. 2(b). By increasing the number of graphene layers coated with modified PEDOT:PSS, the sheet resistance is reduced by as much as 28%. The power conversion efficiency (PCE) values for the two- and five-layer graphene devices are found to be 1.78% and 3.19%, respectively, showing a significant improvement with the increasing number of graphene layers up to five. This result is relatively much improved even without any additional doping process, when compared to the previously reported results with similar device structure where additional doping process has been carried out [18,30]. The performance of OPV with graphene stacked over 5 layers is expected to be diminished. As the number of graphene layer is increased further, the sheet resistance is not effectively improved to enhance the performance compared to degradation in optical transmittance because additional graphene reduces the transmittance linearly by 2.3%. The OPV with the five-layer graphene electrode shows the best output parameters (e.g., fill factor and efficiency) among all of the devices, as shown in Table 1. Moreover, the advantageous effects of the Triton X-100-treated PEDOT:PSS on the wettability and the electrical properties are also confirmed by the output characteristics of the OPVs. Further, to compare

**Table 1 – Summarized organic photovoltaic results of each parameter depending on the number of graphene electrode.**

Type	J <sub>sc</sub> (mA/cm <sup>2</sup> )	V <sub>oc</sub> (V)	FF	Efficiency (%)
2L	7.84	0.547	0.417	1.78
3L	9.90	0.555	0.407	2.13
4L	11.24	0.550	0.410	2.49
5L	12.48	0.563	0.454	3.19

the coating and doping effects on the cell parameters, five-layer pristine graphene electrodes were doped and treated using four different strategies: five-layer graphene treated (a) with pure PEDOT:PSS; (b) with UV treatment and pure PEDOT:PSS; (c) with UV treatment, pure PEDOT:PSS, and doped with nitric acid; and (d) with PEDOT:PSS modified by Triton X-100. These are plotted with black, green, blue and red lines, respectively, as shown in Fig. 5(c). The parameters of flexible OPVs fabricated using these four different methods are summarized in Table 2. It is confirmed that OPVs with Triton X-100-treated PEDOT:PSS show superior output parameters compared to the OPVs using pure PEDOT:PSS. These improvements are due to the lower conductivity in the case of pure PEDOT:PSS, which is caused by the poor interface between the hole transport layer and the graphene electrode; this

**Table 2 – Summarized organic photovoltaic results of each parameter of various methods to improve the efficiency.**

Type	Jsc (mA/cm <sup>2</sup> )	Voc (V)	FF	Efficiency (%)
G/PEDOT:PSS	6.08	0.522	0.402	1.13
UV treated G/PEDOT:PSS	6.90	0.532	0.448	1.65
HNO <sub>3</sub> doped G/PEDOT:PSS	9.43	0.531	0.424	1.98
G/Triton-X PEDOT:PSS	12.48	0.563	0.454	3.19

lowers the number of collected excitons. The short circuit current density and the fill factor, which are directly related to the amount of collected excitons, are both low. The current density and fill factor have been improved for the graphene coated with the modified PEDOT:PSS, as compared to the devices utilizing nitric acid doping, due to enhancement of the doping and the interface between the PEDOT:PSS and the graphene. The UV-treated graphene electrode-based OPV has a better fill factor compared to the non-treated graphene electrode OPV. However, the UV treatment degrades the graphene surface and negatively influences the electrical properties. Therefore, the other parameters, especially the current density, are lower as compared to the other devices. Moreover, a relatively small change in open circuit voltage (OCV) (~0.04V) has been observed in case of Triton X-100/PEDOT:PSS based OPV [22,24]. This is associated with the improvement in the electrical property and the coatibility because the OCV is related to efficient extraction of the holes and electrons, and the difference in work function between hole transport layer (PEDOT:PSS) and electron transport layer (Ca). Finally, the graphene electrode with the Triton X-100-modified PEDOT:PSS coating shows the best performance and is considered to represent the most efficient way to obtain high-performance OPVs as compared to the other techniques.

In order to understand the effect of Triton X-100 treatment on electrical properties in detail, we have collected and analyzed the impedance spectra of both PEDOT:PSS non-treated and treated with Triton X-100 based OPV. The impedance spectroscopy which is generally used to investigate the impedance of each layer and the interface is conducted and the results are shown in Fig. 5(d) [31,32].

Fig. 5(d) shows the diameter of the large semicircle, which is corresponding to Triton X-100 treated PEDOT:PSS based OPV, is significantly larger than that of non-treated PEDOT:PSS based OPV, which is attributed to lower internal resistance for charge transfer events at the donor/acceptor interfaces. The maximum resistance (low frequency x-intercept) shows the value of 3.5 kΩ in the case of non-treated PEDOT:PSS, which reduces to 1.3 kΩ after treating PEDOT:PSS with Triton X-100, due to the improvement in uniform coating over hydrophobic graphene surface. The equivalent circuit for impedance spectra is shown in inset of Fig. 5(d). The arc toward higher frequency side is represented by the combination of  $R_1$  and  $C_1$  which are corresponding to the bulk resistance and capacitance, respectively. The lower frequency side arc represented by  $R_2$  and constant phase element (CPE) is related to the charge transfer resistance between donor/acceptor interfaces, where CPE describes the deviation from ideal capacitance due to the roughness or materials of the

electrodes. Before treating PEDOT:PSS, the resistance value,  $R_1$  and  $R_2$  are 3.2 and 1.2 kΩ, which reduces to 1.24 and 0.40 kΩ, respectively after treating with Triton X-100. Thus, lowering of resistance values further confirms the improvement in electrical properties of whole device due to the uniform coating and doping effect after treating the PEDOT:PSS with Triton X-100.

#### 4. Conclusions

In this study, we have successfully overcome the problem associated with coating an aqueous PEDOT:PSS solution (as a hole transport layer) on a hydrophobic graphene electrode. Having solved this problem by modifying the aqueous PEDOT:PSS solution via the addition of a non-ionic surfactant (Triton X-100), the effects of Triton X-100-treated PEDOT:PSS on the graphene electrode were systematically examined. In addition to forming a uniform coating on the hydrophobic surface, the aqueous PEDOT:PSS simultaneously doped the graphene electrode without an additional wet doping process. Electrical and optical measurements, in addition to the output parameters of OPVs (e.g., the fill factor and short circuit current), demonstrate the positive effects of the modified PEDOT:PSS as both a coating and a dopant. Under optimized conditions, we have fabricated OPVs improved with our graphene electrodes that have a maximum power conversion efficiency of 3.19%; this value is comparable to ITO-based OPVs.

#### Acknowledgements

This work was supported by the National Research Foundation of Korea (NRF) grants Funded by the Korean Government (2012R1A2A1A03006049).

#### Appendix A. Supplementary data

Supplementary data associated with this article can be found, in the online version, at <http://dx.doi.org/10.1016/j.carbon.2014.12.101>.

#### REFERENCES

- [1] Novoselov KS, Geim AK, Morozov S, Jiang D, Zhang Y, Dubonos S, et al. Electric field effect in atomically thin carbon films. *Science* 2004;306:666–9.
- [2] Geim AK, Novoselov KS. The rise of graphene. *Nat Mater* 2007;6:183–91.

- [3] Bae S, Kim H, Lee Y, Xu X, Park J-S, Zheng Y, et al. Roll-to-roll production of 30-inch graphene films for transparent electrodes. *Nat Nanotechnol* 2010;5:574–8.
- [4] Ruiz-Vargas CS, Zhuang HL, Huang PY, van der Zande AM, Garg S, McEuen PL, et al. Softened elastic response and unzipping in chemical vapor deposition graphene membranes. *Nano Lett* 2011;11:2259–63.
- [5] Lee C, Wei X, Kysar JW, Hone J. Measurement of the elastic properties and intrinsic strength of monolayer graphene. *Science* 2008;321:385–8.
- [6] Kim KS, Zhao Y, Jang H, Lee SY, Kim JM, Kim KS. Large-scale pattern growth of graphene films for stretchable transparent electrodes. *Nature* 2009;457:706–10.
- [7] Kavan L, Yum J-H, Graetzel M. Graphene-based cathodes for liquid-junction dye sensitized solar cells: electrocatalytic and mass transport effects. *Electrochim Acta* 2014;128:349–59.
- [8] Ahmad S, Guillen E, Kavan L, Gratzel M, Nazeeruddin MK. Metal free sensitizer and catalyst for dye sensitized solar cells. *Energy Environ Sci* 2013;6:3439–66.
- [9] Jun GH, Jin SH, Lee B, Kim BH, Chae W-S, Hong SH, et al. Enhanced conduction and charge-selectivity by N-doped graphene flakes in the active layer of bulk heterojunction organic solar cells. *Energy Environ Sci* 2013;6:3000–6.
- [10] Robaey P, Bonaccorso F, Bourgeois E, D’Haen J, Diercks W, Dexters W, et al. Enhanced performance of polymer:fullerene bulk heterojunction solar cells upon graphene addition. *Appl Phys Lett* 2014;105: 083306-1.
- [11] Jiang Q, Ao Z, Chu D, Jiang Q. Reversible transition of graphene from hydrophobic to hydrophilic in the presence of an electric field. *J Phys Chem C* 2012;116:19321–6.
- [12] Kim Y-T, Lee S-K, Kim K-S, Kim YH, Ahn J-H, Kwon Y-U. Uniform Growth of high-quality oxide thin films on graphene using a CdSe quantum dot array seeding layer. *ACS Appl Mater Interfaces* 2014;6:13015–22.
- [13] Wang S, Zhang Y, Abidi N, Cabrales L. Wettability and surface free energy of graphene films. *Langmuir* 2009;25:11078–81.
- [14] Park H, Rowehl JA, Kim KK, Bulovic V, Kong J. Doped graphene electrodes for organic solar cells. *Nanotechnology* 2010;21:505204.
- [15] Kim H, Bae S-H, Han T-H, Lim K-G, Ahn J-H, Lee T-W. Organic solar cells using CVD-grown graphene electrodes. *Nanotechnology* 2014;25:014012.
- [16] Wang Y, Chen X, Zhong Y, Zhu F, Loh KP. Large area, continuous, few-layered graphene as anodes in organic photovoltaic devices. *Appl Phys Lett* 2009;95:063302.
- [17] Vosgueritchian M, Lipomi DJ, Bao Z. Highly conductive and transparent PEDOT: PSS films with a fluorosurfactant for stretchable and flexible transparent electrodes. *Adv Funct Mater* 2012;22:421–8.
- [18] Kim K, Bae S-H, Toh CT, Kim H, Cho JH, Whang D, et al. Ultrathin organic solar cells with graphene doped by ferroelectric polarization. *ACS Appl Mater Interfaces* 2014;6:3299–304.
- [19] Park H, Brown PR, Bulović V, Kong J. Graphene as transparent conducting electrodes in organic photovoltaics: studies in graphene morphology, hole transporting layers, and counter electrodes. *Nano Lett* 2011;12:133–40.
- [20] Pan Z, Gu H, Wu M-T, Li Y, Chen Y. Graphene-based functional materials for organic solar cells. *Opt Mater Exp* 2012;2:814–24.
- [21] Wang Y, Tong SW, Xu XF, Özyilmaz B, Loh KP. Interface engineering of layer-by-layer stacked graphene anodes for high-performance organic solar cells. *Adv Mater* 2011;23:1514–8.
- [22] Oh JY, Shin M, Lee JB, Ahn J-H, Baik HK, Jeong U. Effect of PEDOT nanofibril networks on the conductivity, flexibility and coatability of PEDOT:PSS films. *ACS Appl Mater Interfaces* 2014;6:6954–61.
- [23] Liu Z, Li J, Sun Z-H, Tai G, Lau S-P, Yan F. The application of highly doped single-layer graphene as the top electrodes of semitransparent organic solar cells. *ACS Nano* 2011;6:810–8.
- [24] Lee BH, Lee J-H, Kahan YH, Kim N, Kim YJ, Lee J, et al. Graphene-conducting polymer hybrid transparent electrodes for efficient organic optoelectronic devices. *Adv Funct Mater* 2014;24:1847–56.
- [25] Wei P, Liu N, Lee HR, Adjianto E, Ci L, Naab BD, et al. Tuning the dirac point in CVD-Grown graphene through solution processed n-type doping with 2-(2-Methoxyphenyl)-1,3-dimethyl-2,3-dihydro-1 H-benzimidazole. *Nano Lett* 2013;13:1890–7.
- [26] Liu W, Tran XA, Liu X, Wei J, Yu H, Sun X. Characteristics of a single-layer graphene field effect transistor with UV/Ozone treatment. *Electrochem Solid State Lett* 2013;2:M1–4.
- [27] Farmer DB, Golizadeh-Mojarad R, Perebeinos V, Lin YM, Tulevski GS, Tsang JC, et al. Chemical doping and electron-hole conduction asymmetry in graphene devices. *Nano Lett* 2009;9:388–92.
- [28] Kim KK, Reina A, Shi Y, Park H, Li L-J, Lee YH, et al. Enhancing the conductivity of transparent graphene films via doping. *Nanotechnology* 2010;21:285205.
- [29] Gunes F, Shin H-J, Biswas C, Han GH, Kim ES, Chae SJ, et al. Layer-by-layer doping of few-layer graphene film. *ACS Nano* 2010;4:4595–600.
- [30] Lee S, Yeo J-S, Ji Y, Cho C, Kim D-Y, Na S-I, et al. Flexible organic solar cells composed of P3HT:PCBM using chemically doped graphene electrodes. *Nanotechnology* 2012;23:344013.
- [31] Nowy S, Ren W, Wagner J, Weber JA, Brütting W. Impedance spectroscopy of organic hetero-layer OLEDs as a probe for charge carrier injection and device degradation. *Proc SPIE Int Soc Opt Eng* 2009;7415:74150G.
- [32] Leever BJ, Bailey CA, Marks TJ, Hersam MC, Durstock MF. In situ characterization of lifetime and morphology in operating bulk heterojunction organic photovoltaic devices by impedance spectroscopy. *Adv Energy Mater* 2012;2:120–8.